

**Best Estimate HELIOS/DRAGON/NESTLE Codes' Simulation
of a LOCA Power Pulse for a Simplified CANDU-6 Core**

Hisham N. Sarsour
Independent Consultant
1114 Nottingham Circle
Cary, NC 27511
HishamSarsour@cs.com

Paul J. Turinsky
North Carolina State University
Raleigh, NC 27695-7909
turinsky@eos.ncsu.edu

Farzad Rahnema and Scott Mosher
Georgia Institute of Technology
Atlanta, GA 30332
farzad.rahnema@nre.gatech.edu and gt3522a@prism.gatech.edu

Dumitru Serghiuta
Canadian Nuclear Safety Commission
280 Slater Street, 7th Floor
Ottawa, Ontario K1P 5S9
serghiutad@cnsccsn.gc.ca

Guy Marleau and Tanguy Courau
Ecole Polytechnique de Montreal
P.O. Box 6079 , station Centre-ville
Montreal, Quebec H3C 3A7
guy.marleau@polymtl.ca

Introduction

A simplified CANDU-6 model has been established for code-to-code comparison of simulations of a LOCA induced transient. The transient is initiated from steady state initial conditions and originates from a 100% pump suction break under design-centered operating conditions and systems' performance. This results in coolant voiding, the voiding occurring in half the core, with this half core voided in a checkerboard pattern. Voiding progresses at a rate consistent with a LOCA blow down event. which due to the negative coolant density coefficient causes a core transient. The SORs are inserted into the core as a result of an automatic trip signal, which terminates the core neutronics transient. The work presented in this paper has been carried out with the NESTLE core simulator [1]. This work was part of a project sponsored by the Canadian Nuclear Safety Commission (CNSC). The purpose of the project was to gather information and assess the accuracy of best estimate methods using calculation methods and codes developed independently from the CANDU industry.

Simulation Results

The NESTLE core simulator solves the two-group neutron diffusion equation utilizing either a finite difference method or nodal method at the user's discretion. Homogenized cross sections input to NESTLE for this simulation were provided by the HELIOS code [2] with incremental cross sections provided by the DRAGON code [3] based upon HELIOS generated cross sections. The local thermal-hydraulic conditions and trip time were postulated. Specifically, the core thermal-hydraulic conditions that were input to NESTLE as a function of time were determined by the CATHENA code [4]. The time of initial and complete insertion for the SORs, respectively, 0.5615 sec and 1.7115 sec, were based on predictions of CERBERUS/CATHENA simulation of this LOCA transient. The transient was simulated for up to 5.0 sec using NESTLE. The core's burnup distribution was postulated but representative of actual core burnup conditions.

A simplified CANDU6 model has been used for this study. Figure 1 shows the full core mesh layout where 2 indicates a fuel node, 1 a reflector node, and 0 a null node. This model has 380 channels with 12 bundles in each channel. The maximum number of channels in the x and y directions is 22. The lattice pitch is 28.575 cm and the bundle length is 49.53 cm. The base spatial mesh is 42x34x22 (x,y,z). The radial reflector's minimum thickness is 68.525 cm and the notch is not modeled. There is no reflector in the axial direction. The boundary condition is zero flux on all external surfaces, with the radial boundary treated by a Cartesian raggedy edge in the D₂O reflector. Adjuster rods and zone control units states are held fixed at their initial conditions throughout the transient.

Reactivity drivers for the LOCA transient are the core's thermal-hydraulic conditions. The CATHENA code predicts that the volume average coolant density decreases from 0.82 gm/cc to 0.09 gm/cc in the broken pass, and from 0.82 gm/cc to 0.30 gm/cc over the total core, providing substantial positive reactivity due to the negative coolant density reactivity coefficient. The volume average fuel temperature is predicted to increase from 598.6 °C to a maximum of 660.3 °C in the broken pass, and from 595.5 °C to a maximum of 643.9 °C over the total core, implying a very mild fuel temperature transient and hence very mild reactivity effect.

The k_{eff} values for the initial steady state core condition as predicted by NESTLE finite difference method (FDM), NESTLE nodal method (NM) without assembly discontinuity factors (ADF), and NESTLE NM with ADF are 1.00249, 1.00134, and 1.00274. Refining the spatial mesh case by halving the spatial mesh spacing in all directions, the k_{eff} values as predicted by NESTLE FDM and NESTLE NM with ADF were reduced by 0.19 mk and 0.18 mk, respectively, from the values utilizing the original spatial mesh. This indicates that even using the NM that k_{eff} was not accurately predicted due to spatial discretization errors.

Table I shows the time-step sizes used for the base case. Other cases with finer time-step sizes are based upon uniform refinements of the time-step sizes that are in Table I. Figure 2 shows the total prompt thermal power transient as predicted by NESTLE

utilizing the three different spatial discretization treatments for the base case time-step sizes. Note that the fission source term in NESTLE is scaled by $1/k_{eff}$, so the differences in the predicted initial k_{eff} value due to spatial discretization treatment are effectively removed. The peak powers, noted to occur at 0.7795 sec for all three spatial discretization treatments, are predicted to be 218.81%FP, 213.95%FP, and 216.73%FP for FDM, NM without ADF, and NM with ADF, respectively. The differences are very small given the severity of the core's transient.

Figure 3 presents the total prompt thermal power transient as predicted by NESTLE NM with ADF employing finer time-step sizes. The finer time-step sizes are constructed by taking $\frac{1}{2}$, $\frac{1}{4}$, and $\frac{1}{10}$ of the original time-step sizes. The peak power does not change much with time-step size refinement, with values of 215.22%FP, 214.93%FP, and 214.79%FP for $\frac{1}{2}$, $\frac{1}{4}$, and $\frac{1}{10}$, respectively, refinements of the original time-step sizes. This is to be compared with a peak power value of 216.73%FP predicted using the original time-step sizes. It is also clear that the total prompt thermal power is predicted to rise faster up to the peak power value for the original time-step sizes when compared with the finer time-step sizes.

Figure 4 contrasts the total prompt thermal power transient for NESTLE FDM and NESTLE NM with ADF employing the refined (halved) spatial mesh. The peak power as predicted by NESTLE NM with ADF (217.57%FP) is about 1.5% higher than that as predicted by NESTLE FDM (216.16%FP). Note that the peak power as predicted by NESTLE FDM using the refined spatial mesh is noted to be 2.65%FP lower than that predicted using the original spatial mesh; however, NESTLE NM with ADF displays the reverse behavior in that using the refined spatial mesh results in a 0.84%FP higher peak power being predicted than that predicted using the original spatial mesh. The smaller change in peak power with spatial mesh refinement observed for NESTLE NM versus NESTLE FDM is consistent with the NM leading to reduced spatial discretization errors.

The top ten bundles and channels with regard to energy deposited over the transient are shown in Table II and Table III, respectively. The differences in energy deposited, whether on a bundle or channel basis, between the FDM and NM with ADF, are at most 3%. These three spatial discretization methods do not always predict the same rank ordering of bundles, but the differences in energy deposited as a function of ranking are small, so the changes in rank ordering are not significant.

Total energy deposited during the 5 seconds is 4301.3 Mjoule for FDM, 4198.9 Mjoule for NM without ADF, and 4208.9 Mjoule for NM with ADF.

Conclusions

The total prompt thermal power transient induced by a LOCA transient has been determined to be insensitive to the spatial discretization treatment utilized in NESTLE for a simplified CANDU-6 model. The same conclusion is reached with regard to the bundle and channel energy deposited over the transient.

References

- [1] P. J. Turinsky, R. M. K. Al-Chalabi, P. Engrand, H. N. Sarsour, F. X. Faure and W. Guo, "NESTLE: A Few-Group Neutron Diffusion Solver Utilizing the Nodal Expansion Method for Eigenvalue, Adjoint, Fixed-Source Steady-State and Transient Problems," EGG-NRE-11406, Idaho National Engineering Laboratory (1994).
- [2] Casal J J, Stamm'ler R J J, Villarino E A and Ferri A A, "HELIOS: Geometric Capabilities of a New Fuel-Assembly Program," Intl Topical Meeting on Advances in Mathematics, Computations, and Reactor Physics, Pittsburgh, Pennsylvania, April 28-May 2, 1991, Vol. 2, p. 10.2.1 1-13 (1991).
- [3] R. Roy, G. Marleau, J. Tajmouati and D. Rozon, "Modeling of CANDU Reactivity Control Devices with the Lattice Code DRAGON," Ann. Nucl. Energy, **21**, 115 (1994).
- [4] B.N. Hanna ed, "CATHENA Abstract MOD-3.5c/Rev 0", COG-99-6, 1999

Table I. Original time-step sizes used for the base case

Time Span That Time-step Size Is Applied To		Time-step Size (sec)
Starting Time (sec)	Ending Time (sec)	
0.0	0.5	0.1
0.5615	2.0	0.036-0.107
3.0	5.0	1.0

**Table II. Top ten bundles with regard to energy deposited over the transient.
(Bundle Energy Addition=Time integrated power from start to end of transient)**

Bundle Ranking	Method	Energy (KJoule/Kg)	Location (Radial, Axial)
1	FDM	119.8	(P5, 6)
	NM w/ ADF	118.1	(P5, 6)
	NM w/o ADF	118.4	(P5, 6)
2	FDM	119.1	(P5, 7)
	NM w/ ADF	117.4	(P5, 7)
	NM w/o ADF	117.7	(P5, 7)
3	FDM	118.6	(S10, 6)
	NM w/ ADF	116.6	(Q6, 6)
	NM w/o ADF	116.5	(Q6, 6)
4	FDM	118.5	(Q6, 6)
	NM w/ ADF	116.5	(R7, 6)
	NM w/o ADF	116.1	(R7, 6)
5	FDM	118.3	(R7, 6)
	NM w/ ADF	115.8	(O6, 6)
	NM w/o ADF	115.6	(Q6, 7)
6	FDM	118.0	(S10, 7)
	NM w/ ADF	115.7	(Q6, 7)
	NM w/o ADF	115.2	(R7, 7)
7	FDM	117.7	(O6, 6)
	NM w/ ADF	115.6	(R7, 7)
	NM w/o ADF	114.6	(O4, 6)
8	FDM	117.6	(Q6, 7)
	NM w/ ADF	115.4	(S10, 6)
	NM w/o ADF	114.1	(O6, 6)
9	FDM	117.4	(R7, 7)
	NM w/ ADF	115.0	(O6, 7)
	NM w/o ADF	114.1	(O4, 7)
10	FDM	116.9	(O6, 7)
	NM w/ ADF	114.7	(S10, 7)
	NM w/o ADF	113.8	(S10, 6)

**Table III. Top ten channels with regard to energy deposited over the transient.
 (Channel Energy Addition=Time integrated power from start to end of transient)**

Channel Ranking	Method	Energy (MJoule)	Location
1	FDM	17.9500	O6
	NM w/ ADF	17.6226	O6
	NM w/o ADF	17.4545	P5
2	FDM	17.8915	S10
	NM w/ ADF	17.4655	R7
	NM w/o ADF	17.4379	O4
3	FDM	17.8633	O4
	NM w/ ADF	17.4525	P5
	NM w/o ADF	17.3461	R7
4	FDM	17.8260	S9
	NM w/ ADF	17.4393	R8
	NM w/o ADF	17.3139	O6
5	FDM	17.8000	R7
	NM w/ ADF	17.4034	S10
	NM w/o ADF	17.1531	R8
6	FDM	17.7892	R8
	NM w/ ADF	17.3508	S9
	NM w/o ADF	17.1394	M4
7	FDM	17.7643	P5
	NM w/ ADF	17.3481	O4
	NM w/o ADF	17.1309	S10
8	FDM	17.6223	M4
	NM w/ ADF	17.2883	R9
	NM w/o ADF	17.0760	S9
9	FDM	17.5207	Q7
	NM w/ ADF	17.2033	Q7
	NM w/o ADF	16.9834	S8
10	FDM	17.4632	R9
	NM w/ ADF	17.1411	M4
	NM w/o ADF	16.9536	R9

Figure 1. Full core mesh layout where 2 indicates a fuel node, 1 a reflector node, and 0 a null node

```
0000000000000000000011111100000000000000000000000000
000000000000001111111111111111111100000000000000000
0000000001111111111111111111111111111100000000000
00000001111111111111111111111111111111111000000000
000000111111111122222222222222221111111111110000000
0000011112222222222222222222222222222221111000000
0000111222222222222222222222222222222222211100000
000111222222222222222222222222222222222221110000
001112222222222222222222222222222222222221110000
001112222222222222222222222222222222222221110000
001112222222222222222222222222222222222221110000
001112222222222222222222222222222222222221110000
011122222222222222222222222222222222222221110000
011122222222222222222222222222222222222221110000
011222222222222222222222222222222222222221110000
011222222222222222222222222222222222222221110000
111222222222222222222222222222222222222221110000
111222222222222222222222222222222222222221110000
111222222222222222222222222222222222222221110000
111222222222222222222222222222222222222221110000
011222222222222222222222222222222222222221110000
011222222222222222222222222222222222222221110000
011122222222222222222222222222222222222221110000
011122222222222222222222222222222222222221110000
001112222222222222222222222222222222222221110000
001112222222222222222222222222222222222221110000
001112222222222222222222222222222222222221110000
000111222222222222222222222222222222222221110000
0000111222222222222222222222222222222222211100000
00000111112222222222222222222222222222221111000000
000000111111111122222222222222222222222211111000000
0000000111111111111111111111111111111111100000000
000000000111111111111111111111111111111111100000000
000000000000111111111111111111111111111100000000000
000000000000000000000011111110000000000000000000000
```

Figure 2. Total prompt thermal power (%) versus time for simplified CANDU-6 problem

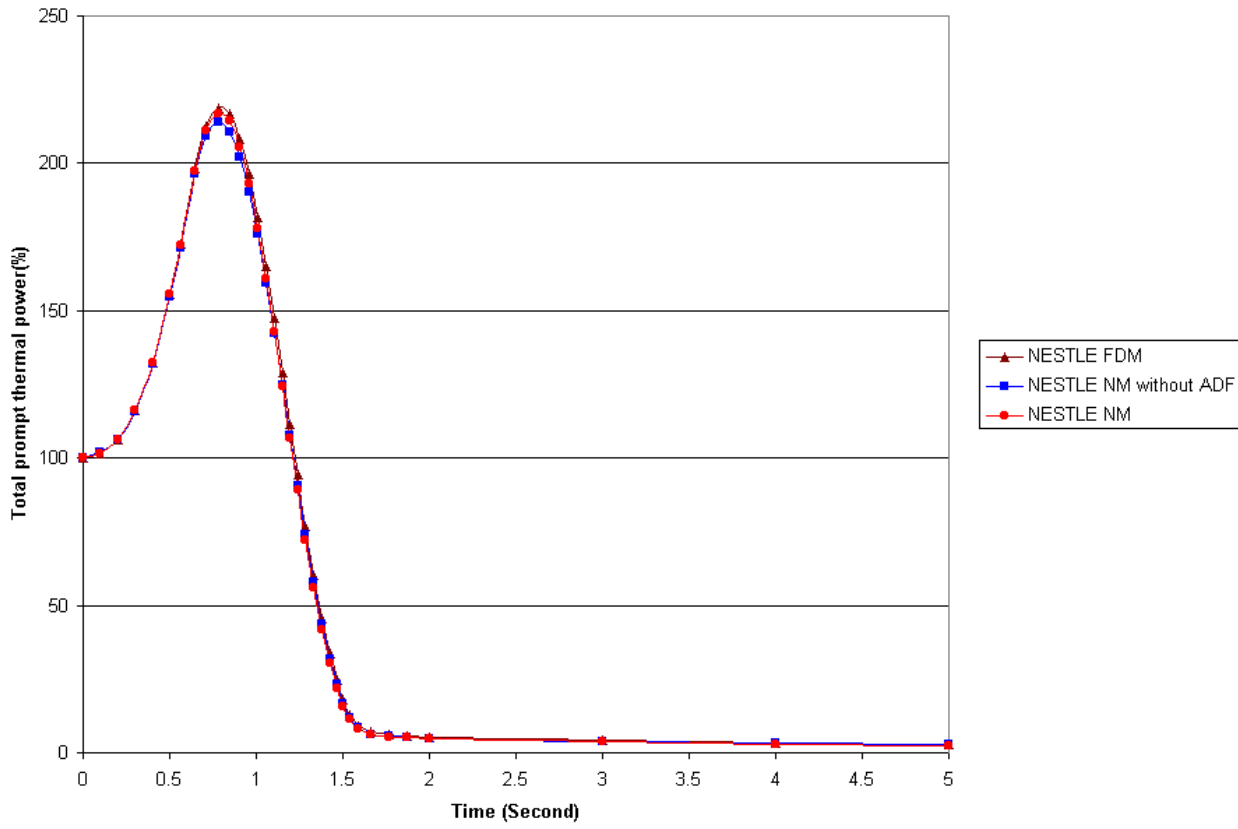


Figure 3. Total prompt thermal power (%) versus time for simplified CANDU-6 problem for different time-steps utilizing NESTLE NM with ADF

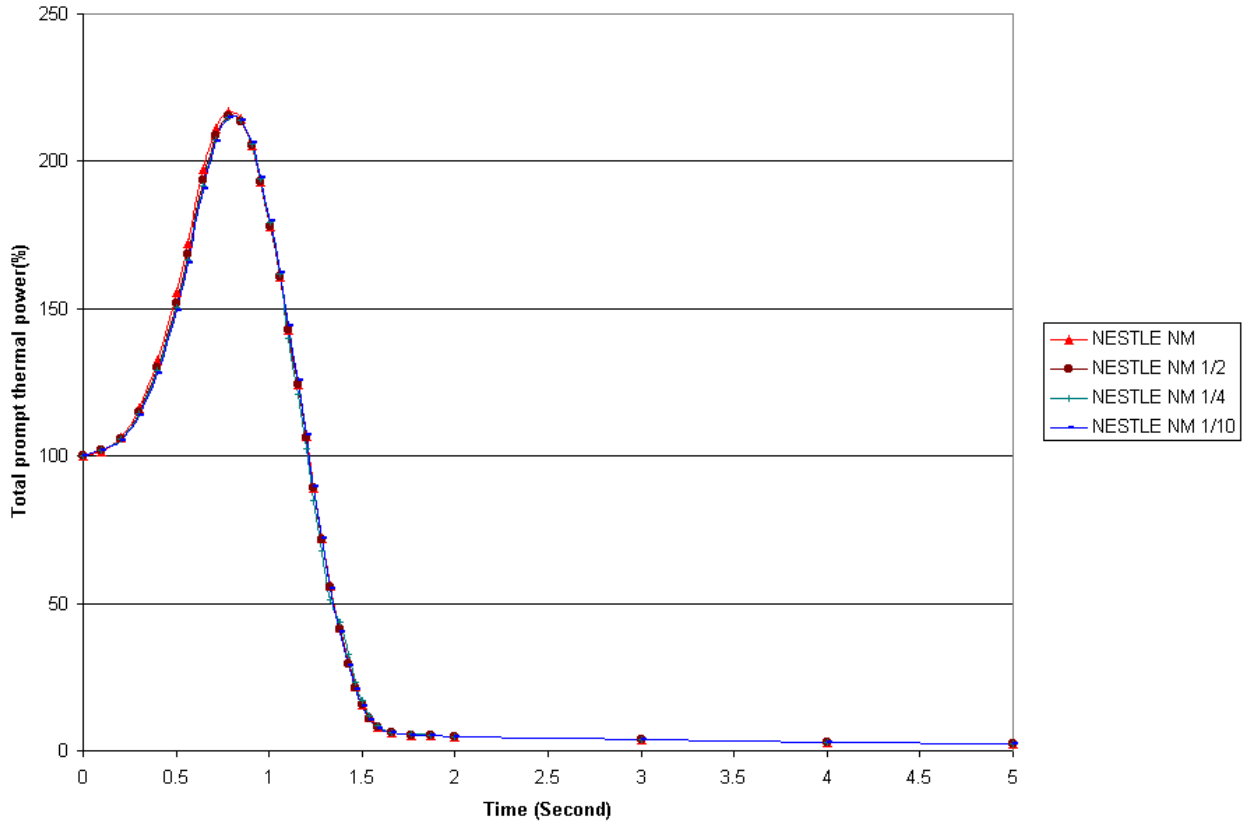


Figure 4. Total prompt thermal power (%) versus time for simplified CANDU-6 problem for original and refined spatial meshes

